UNIVERSITY OF TWENTE.

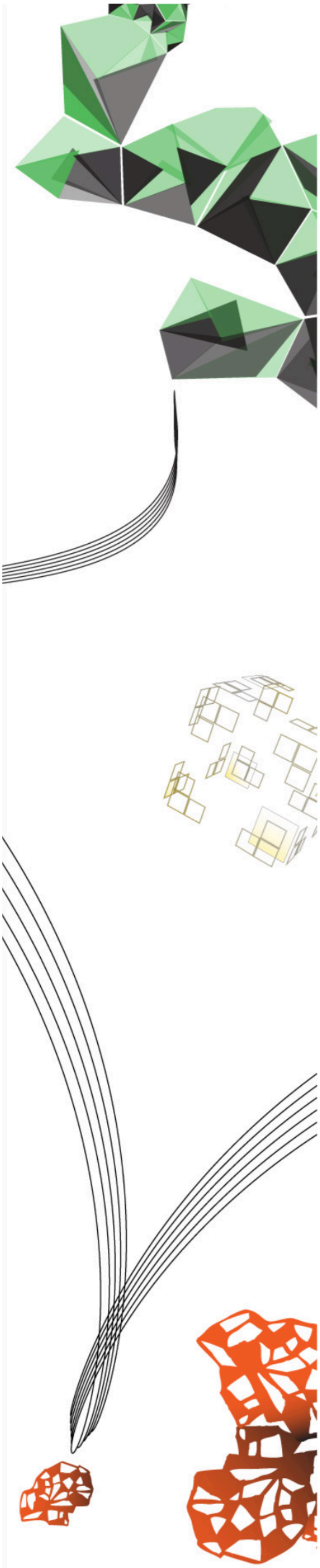

# PATTERNING POROUS CATALYST USING WETTABILITY CONTRAST AND KINETIC STUDY OF FRUCTOSE DEHYDRATION

Jing Li

FACULTY OF SCIENCE AND TECHNOLOGY (TNW)
SFI GROUP
CHAIRMAN: PROF.DR.IR. R.G.H. LAMMERTINK

**EXAMINATION COMMITTEE**
PROF.DR.IR. R.G.H. LAMMERTINK
PROF.DR.IR. A.J.A. WINNUBST
MSc. A. VISAN

# Abstract

Biomass is drawing more and more attention as a sustainable and environmental-friendly energy resource. As fructose being one of the main components of agricultural waste, various catalysts have been developed to convert fructose into useful chemicals. While most of these catalysts are particles, the kinetic process and mass transfer are still unknown. Therefore, we would like to fabricate a microreactor with an immobilized catalyst for fructose conversion to study the kinetics of the process. Dip coating and wash coating were tried to coat a porous catalyst film on the Si substrate. Porous catalyst patterns were fabricated by dip coating using wettability contrast. Ellipsometry and SEM were used to characterize the surface properties of these thin films.

# Contents

# Chapter 1

# Introduction

Biomass is an industry term depicting the material derived from growing plants or animal manure used for energy production. [4] Due to increasing pressing energy and environmental issues, people are looking for sustainable and renewable alternatives to replace the widely used fossil fuels. [5] Biomass can be obtained from various resources such as wood and wood waste, agricultural crops and their waste byproducts, waste from food processing and aquatic plants. [6] Biomass has been mostly used directly by burning, with very low efficiency while releasing large amount of carbon dioxide. Biomass has a high degree of complexity which we can benefit from. It is can be used indirectly by converting it into liquid fuels or various valuable chemicals [7] including 5-hydroxymethylfurfural (HMF), levulinic acid (LA) and $\gamma$-valerolactone (GVL) [8].

HMF is an important intermediate formed from carbohydrates such as glucose or fructose. However, there isn't yet direct commercial production of HMF from fructose or glucose, due to the lack of practical and efficient processing with low energy consumption. [9,10] The challenge for the effective utilization of biomass is to develop novel and ecofriendly catalysts for the efficient transformation at low cost. [11,12] Group VIII metals, notably ruthenium have been shown to facilitate the hydrogenation step in liquefaction. But the cost of these precious metals is too high for large-scale use. Thus, inexpensive heterogeneous catalysts, such as Zirconium dioxide and Titanium dioxide are attracting more and more attention as alternatives. [13]

Watanabe *et al.* used hot compressed water as an environmental-friendly and cheap medium to examine the effect of $TiO_2$ and $ZrO_2$ on the glucose and fructose reactions. Both $ZrO_2$ and $TiO_2$ promoted the dehydration into HMF. [14] Nakajima *et al.* reported a method to significantly enhance the catalytic performance of $TiO_2$ by modifying with phosphoric acid. [15] Hattori *et al.* combined phosphate-immobilization with UV light irradiation and increased the selectivity toward HMF production. [9] Besides improving the intrinsic kinetics by surface functionalization, the overall conversion can also be increased through enhanced mass transfer, by making use of diffusio-osmotic surface flows which are generated by contrast in activity.

In this assignment, we use various routines including wash coating and dip coating to pattern porous $ZrO_2$ and $TiO_2$ inside microchannels in order to study the interfacial transport phenomena. Patterning of porous materials inside microchannels can be achieved using wettability contrast.

# Chapter 2

# Synthesis of Microchannels

## 2.1 Theory

### *2.1.1 Microreactor*

A microreactor is a device with channel dimensions below 1mm in which chemical reactions take place. [16] Microreactors have been used a lot for kinetic study, multiphase reaction engineering and process development for scaling up the catalytic technologies from laboratory scale to pilot-plant systems and eventually to commercial-scale processes. [17] Microreactors can be efficiently used to screen catalytic materials and can provide better energy and material utilization leading to cost reduction and less pollution. [18] Other advantages include improved safety characteristics, enhanced rates of heat and mass transfer and higher chemical conversions. [17,18] For this assignment, well-defined fluid dynamics and visualization techniques are additional benefits for using microreactors.

Figure 2.1 Picture of a microreactor with sputtered $ZrO_2$ layer used in this assignment.

### *2.1.2 Coating with contrast in wettability*

For both wash coating and dip coating methods, particles self assemble on a hydrophilic substrate and form a thin film on top. Experiments have proved that aqueous suspension can selectively wet a patterned substrate with an array of hydrophilic and hydrophobic materials. [19] These two deposition methods should be able to coat particles on a desired region with high resolution.

### *2.1.3 Hydrophobization*

The chemical nature of surfaces including wettability can be altered and controlled by absorbing self-assembled monolayers (SAM) with low surface energies onto solid substrates. [20] For $SiO_2$ surfaces, organosilanes including alkylchlorosilane and alkylalkoxysilane

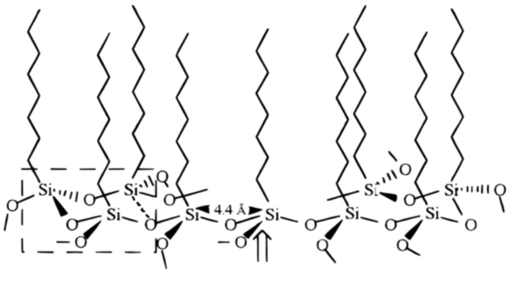

Figure 2.2 Formation and Structure of Self-Assembled Monolayers [1]

are commonly used for assembling into thin monolayers with the formation of cross-linked siloxane bridges (Si-O-Si) between adjacent molecules (Figure 2.2). [1] A tri-functional silane trichloro (1H, 1H, 2H, 2H-perfluorooctyl) silane (FOTS) is used in this assignment to form densely packed monolayers in the microchannels. FOTS is stable up to 400-450°C, which is suited for the following biomass conversion. [21] The principle reaction scheme for FOTS has two steps:

The first step is the hydrolyzation of Cl:

$$C_8H_4F_{13}\text{-}SiCl_3+H_2O \rightarrow C_8H_4F_{13}\text{-}Si\text{-}(OH)_3+3HCl$$

In a second step the hydrolyzed silanes attach to the hydrophilic $SiO_2$ surface and generate strong covalent Si-O bonds with the substrate. [21]

### 2.1.4 Wash coating

Various techniques including cathodic sputtering, spin coating and chemical vapor deposition are commonly used to produce uniform and homogeneous layers in the nm range. However, coatings created by these methods all suffer from low surface area and activity and are not suited as catalysts for chemical reactions. [22] A prominent coating technique for catalysts with high surface area is wash coating. A complete wash coating process consists of surface pretreatment, slurry preparation, slurry deposition and drying and calcination. [22,23] A pretreatment is alternative to be used before coating to improve the adherence. Chemical or thermal pretreatment are most frequently applied, such as basic/acidic treatment [24] and thermal oxidation [25]. Besides pretreatment, the catalyst slurry needs to be prepared. To make the slurry, the catalyst is mixed with solvent and sometimes with binder material such as polyvinyl alcohol or methylhydroxyethyl cellulose. [22] In this project, zirconium dioxide and titanium dioxide suspensions in water are used as slurries without any additives. During the deposition, the slurry is flushed out with air or other gas after the channel is filled. With the hydrophilic/hydrophobic patterns, metal oxide particles in water should only stick to the hydrophilic parts. Calcination is the last step of the process after drying to get rid of the solvent and binders and to strengthen the adhesion of the layer. Repeat wash coating is possible to achieve a larger thickness of the coating.

### 2.1.5 Dip coating

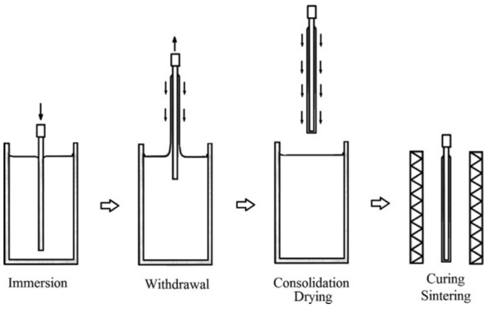

Figure 2.3 Procedure of dip coating. [3]

Dip coating is a simple and traditional technique that can coat thin layers on many kinds of substrates. Dip coating involves of the withdrawal of a substrate from a fluid sol or suspension. A thin solid film is deposited on both sides of the substrate as a result of gravitational draining and solvent evaporation. After deposition, various techniques can be used for characterization such as ellipsometry, scanning electron microscope (SEM) and X-ray powder diffraction (XRD). [26] When drawing up a substrate from a water-based suspension, the particles only selectively coat on the hydrophilic part of the surface. Therefore, particles can be coated on desired regions using hydrophilic/hydrophobic patterns. [19]

## 2.2 Experimental

### *2.2.1 Chemicals:*

Zirconium oxide nanopowder water dispersion ($ZrO_2$, US Research Nanomaterials, 20wt%, 45-55nm), Aqueous dispersion of hydrophilic fumed titanium dioxide ($TiO_2$, Evonik, 29-31wt%, mean aggregate size≤100nm), Trichloro (1H, 1H, 2H, 2H-perfluorooctyl) silane (FOTS, Aldrich), Nitric acid (65%, ACROS), Chromium etchant (Aldrich), Distilled water.

### *2.2.2 Equipment*

Pump (Harvard PHD ULTRA), oven (Heraeus), oven (Navertherm), Dip coater (QPI-128, QUALTECH PRODUCTS INDUSTRY CO. LTD)

### *2.2.3 Procedure:*

(i) Hydrophobization

a) Clean the sample with 65% $HNO_3$ for at least 15min, rinse with distilled water and dry with Nitrogen flow;
b) Put the chip/wafer in the oven, dry for at least 30min at 120°C;
c) Set the temperature to 100°C, pre-heat the setup as well as pipette tip;
d) Add 10μl FOTS to the system, flow with nitrogen for at least 2h.

For large wafers after photolithography, the first cleaning step can be skipped since they are cleaned in the clean room.

(ii) Wash coating

a) Wash the channel once with 65% nitric acid for 15min under a flow rate of 10μl/min (Syringe: Hamilton, 5ml);
b) Flush the channel twice with distilled water to wash away the nitric acid (Syringe: BD, 3ml);

c) Fill the channel with 20wt% $ZrO_2$ suspension under a flow rate of 100µl/min and displace it with air at a certain flow rate;
d) Sinter the chip at 500°C for 2h with a heating rate of 2°C/min.

(iii) Dip coating of small Si wafer for $ZrO_2$ and $TiO_2$

a) Clean the wafer with 65% nitric acid for 15min,
b) Flush the wafer with distilled water and dry with nitrogen flow,
c) Dip coat the wafer at a certain withdrawal rate,
d) Once dry in air, sinter the wafer at 500°C for 2h with a heating rate of 2°C/min.

Eight combinations of different concentration with different withdrawal rate were used for $ZrO_2$ and nine for $TiO_2$.

(iv) Dip coating of large wafer with photoresist patterns

The wafer was directly dip coated after coated with photoresist. Photoresist was then lifted off after sintered at 120°C for 2h. A second calcination step was applied at 500°C for 2h.

(v) Dip coating of large wafer with Cr patterns

The wafer was patterned with Cr by photolithography, then hydrophobized with FOTS. The Cr layer was etched away with Chromium Etchant by keeping the wafer in a petri dish with etchant for around 1 min.

(vi) Dip coating of large wafer with hydrophobic patterns

A layer of photoresist was patterned onto the surface using photolithography in clean room. The photoresist was lifted off after hydrophobization. Then the wafer was dip coated with $TiO_2$ suspension and sintered at 500°C. The hydrophilic patterns, which were coated by photoresist, are now coated with desired catalyst.

## 2.3 Results and discussion

### *2.3.1 Size measurement*

Both sizes of $ZrO_2$ and $TiO_2$ suspensions were measured with a Zetasizer. Zetasizer measures the diffusion of molecules moving under Brownian motion, and converts this to size and size distributions using the Stokes-Einstein relationship. Three distributions were recorded for each measurement and represented by the red, green and blue curves shown in the plots below.

(i) $ZrO_2$ from US RN

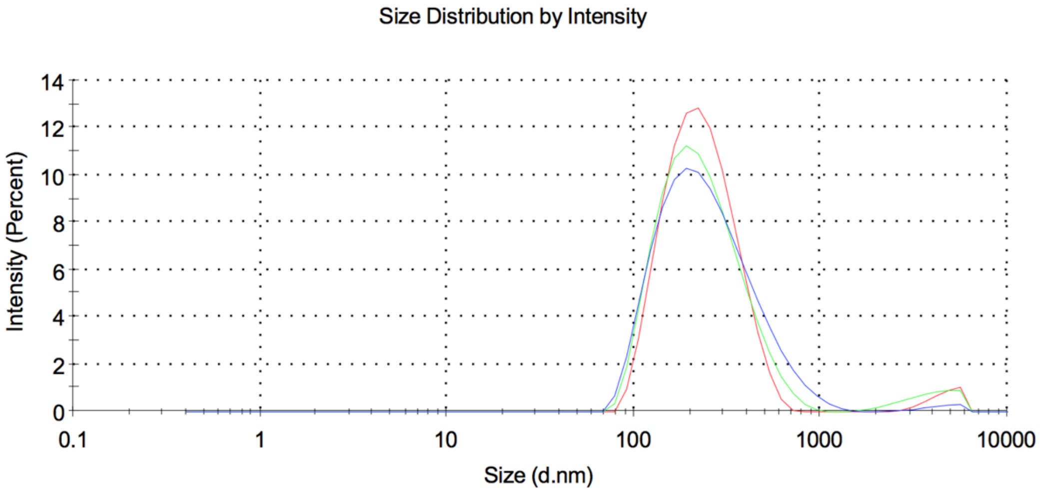

Figure 2.4 Size distribution by intensity of $ZrO_2$ suspension from US RN.

Figure 2.4 is the size distribution plotted by intensity of $ZrO_2$ suspension from US Research Nanomaterials. Particle size of the strongest peak is around 270nm and the small peak around 4400nm might be the signal of some dirt or other large contaminates. The size of these $ZrO_2$ particles varies from 70nm to 1000nm. The expected film thickness for this project is 1μm, and particles of 270nm are too large to form a continuous layer on the substrate.

(ii) $ZrO_2$ from Aldrich

The size of $ZrO_2$ particles from Aldrich was also measured by Zetasizer. There are still a lot of aggregates in this suspension with the average size around 250nm. Since

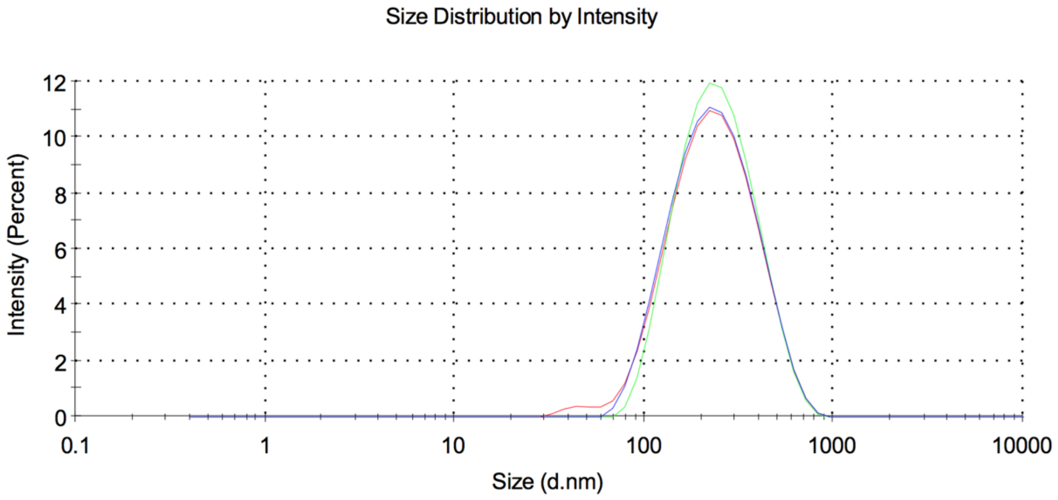

Figure 2.5 Size distribution by intensity of $ZrO_2$ suspension from Aldrich.

small and dispersed particles are a prerequisite for homogeneous layer. Polydispersity given by high degree of aggregation makes these suspensions unsuitable for catalytic film fabrication.

(iii) $TiO_2$ from Evonik

Since $TiO_2$ and $ZrO_2$ have similar structure and are often used for the same reactions, $TiO_2$ suspension from Evonik was also measured with Zetasizer. Figure 4 shows the size distribution by intensity of $TiO_2$ from Evonik. The peak of size is around 150nm, and the minimum size is around 20nm, which is similar to the specifications given by the company.

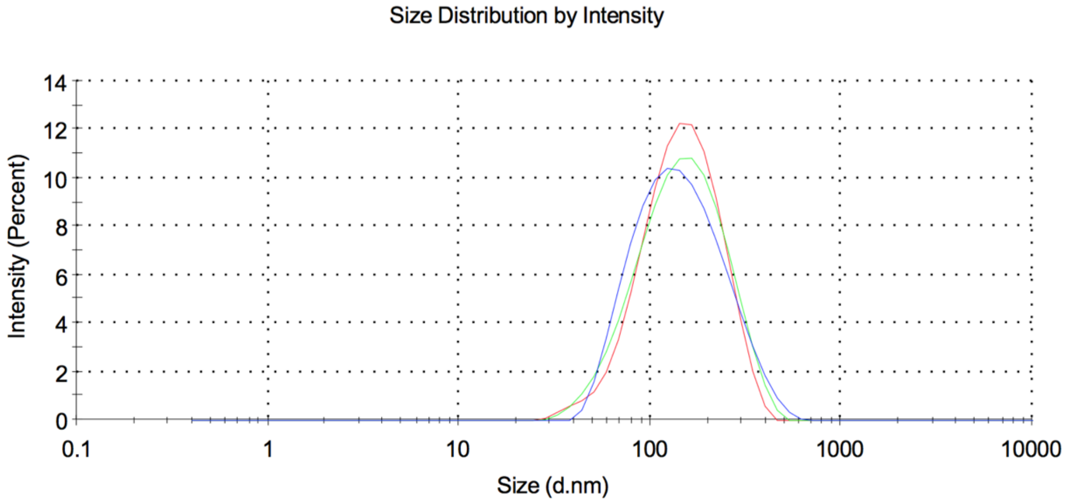

Figure 2.6 Size distribution by intensity of $TiO_2$ suspension from Evonik.

### 2.3.2 Hydrophobization

Four pieces of flat Si wafers were hydrophobized at the same time, and three of them were treated with water, Cr etchant and nitric acid for 15min afterwards. The hydrophobicity of these wafers was measured with contact angle measurement. Three spots were measured for each sample and an average number is calculated.

Table 2.1 Contact angles of water on different samples.

| Wafer | No treatment | Water | Cr etchant | Nitric acid (65%) |
|---|---|---|---|---|
| Average contact angle (degree) | 103.0 | 103.0 | 103.5 | 99.8 |

The hydrophobicity of the wafer after treated with nitric acid decreased significantly while the other three samples have similar hydrophobicity. The FOTS layer might has hydrolyzed in nitric acid solution. Washing with nitric acid is not an appropriate cleaning method for hydrophobized surface.

The wettability of a wafer after dip coating was also measured with contact angle measurement. The hydrophobic parts turned hydrophilic again after sintered at 500°C since the contact angle is only 21.3°. We can either hydrophobize the channel again or use a lower temperature for calcination if a hydrophobic surface is needed.

### *2.3.3 Wash coating inside microreactors*

After wash coating, a thin layer of $ZrO_2$ is left on the bottom of the channel. The catalyst layer is white before calcination. The film is a collection of individual aggregates of different sizes, rather than a continuous layer. The inlet part of the channel, which should be still hydrophobic, is also coated by the suspension.

Figure 2.7 Picture of a chip wash coated with 20wt% $ZrO_2$ suspension.

The catalyst layer turned yellow after calcination. Figure 2.7 shows a microreactor after calcination, catalyst layer does not cover the entire channel continuously and can not be used for further modeling.

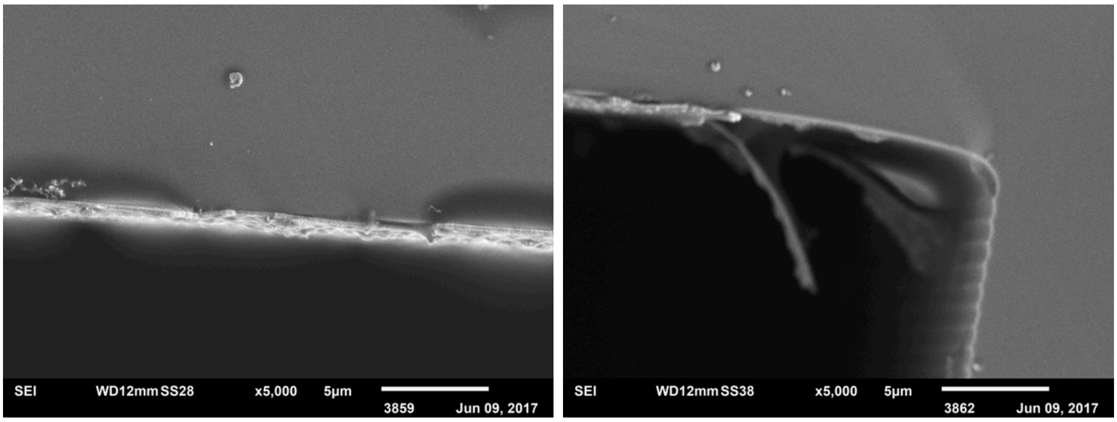

Figure 2.8 Cross sectional SEM images of the channel after wash coating under the magnification of 1) ×5000, 2) ×5000.

We can see from the SEM image that there is a thin layer left at the bottom of the channel. The layer is thinner and not so uniform as what we expected. What's more, the corner of the channel is barely coated by any thing according to the right image.

### *2.3.4 Dip coating on flat Si substrate*

(i) $ZrO_2$

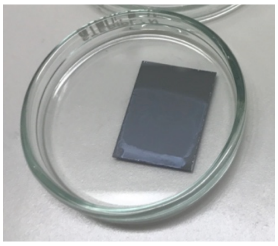

Figure 2.9 Picture of a wafer dip coated with 2wt% $ZrO_2$ suspension at 50mm/min.

After dip coating, both sides of the wafer are coated with a white thin layer. The bottom part is more concentrated because of the gravity force. Figure 2.9 shows a wafer coated by dip coating method with 2wt% $ZrO_2$ suspension at 50mm/min.

After calcination, this wafer was measured with ellipsometry for thickness. However, not as expected, the thickness is only 56.47nm when fitted with a $ZrO_2$ Cauchy model, which is even smaller than the smallest size of $ZrO_2$ particles measured by Zetasizer. As can be seen from the SEM pictures, the surface is covered with aggregates of random sizes and there is barely a layer under the aggregates.

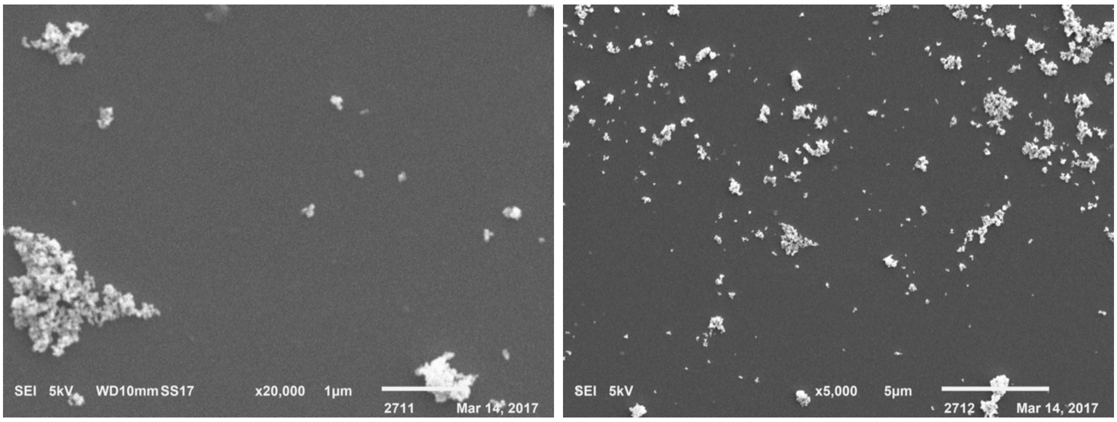

Figure 2.10 SEM images of a wafer dip coated with 2wt% $ZrO_2$ suspension at 50mm/min at ×20000 and ×5000 magnification.

### (ii) $TiO_2$

#### a) Small wafers

After calcination, all the wafers are characterized with ellipsometry with the model of $TiO_2$ Cauchy layer. Each wafer is measured three times and then an average thickness is calculated.

Table 2.2 Average thickness of $TiO_2$ layers dip coated on Si wafer.

| Concentration (wt%) | 5 | | | | |
|---|---|---|---|---|---|
| Withdrawal rate (mm/min) | 50 | | 100 (with graded layer) | 150 | |
| Sample | 1 | 2 | | 1 | 2 |
| Average thickness (nm) | 115.50 | 137.62 | 171.48 | 199.70 | 225.20 |

| Concentration (wt%) | 10 | | 15 | | 30 | |
|---|---|---|---|---|---|---|
| Withdrawal rate (mm/min) | 50 | 100 | 50 | 100 | 10 | 50 |
| Average thickness (nm) | 255.20 | 389.46 | 437.93 | 493.24 | 1071.92 | 1831.00 |

As we can see from the results, the thickness of the layer increase with a higher flow rate as well as higher suspension concentration. To achieve a uniform layer with desired thickness around 1μm, a recipe of 30wt% $TiO_2$ suspension with a withdrawal rate of 10mm/min is used for further experiments.

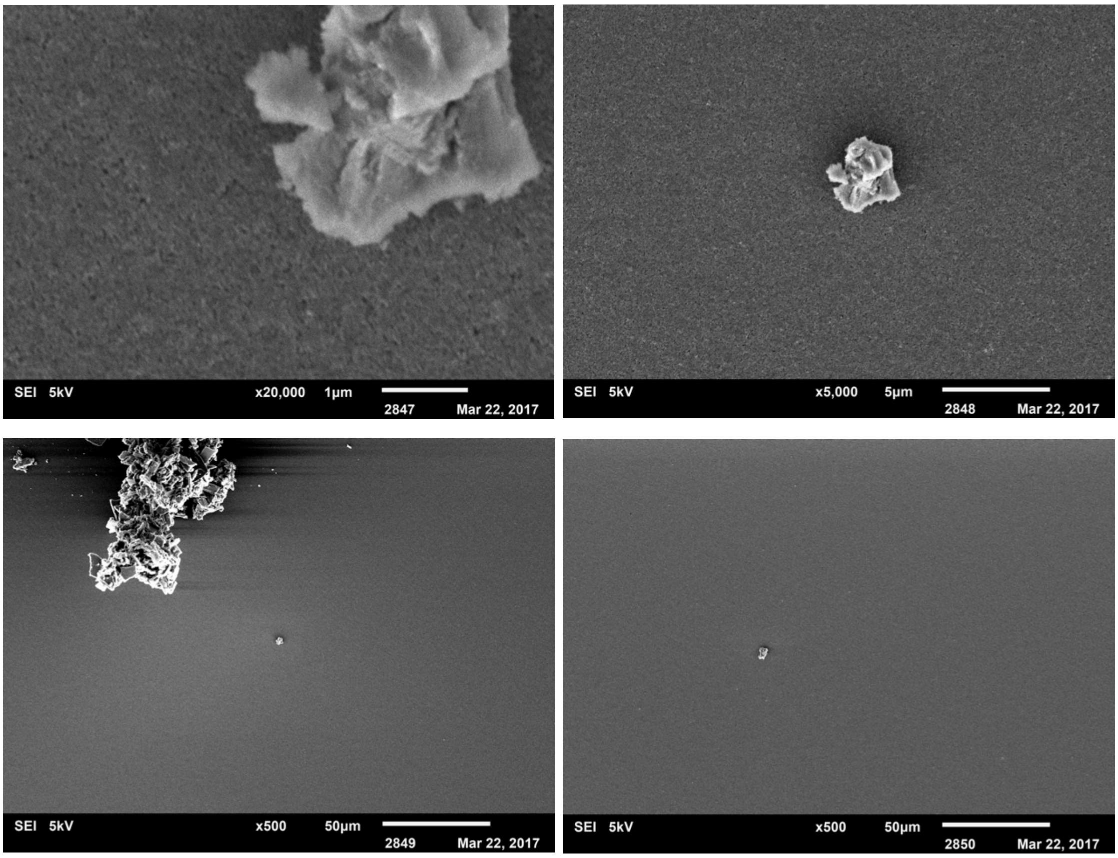

Figure 2.11 SEM images of a wafer dip coated with 30wt% $TiO_2$ suspension at 10mm/min under the magnification of 1) ×20000, 2) ×5000, 3) ×500, 4) ×500

SEM was also used to test the uniformity of the $TiO_2$ surface. From the first picture, which has a magnification of ×20000, we can see that the surface is quite uniform and porous besides some large particles. The $TiO_2$ has some roughness but this roughness can be hardly recognized under the magnification of ×500. The large particles might be some dust, large $TiO_2$ aggregations or some silicon particles attached when breaking the wafers.

b) Selectively patterning $TiO_2$ on Si substrate

Three procedures were tried to selectively pattern $TiO_2$ film on flat Si substrate.

- Photolithography for dip coating
- Photolithography for Cr coating
- Photolithography for hydrophobization

*Photolithography for dip coating*

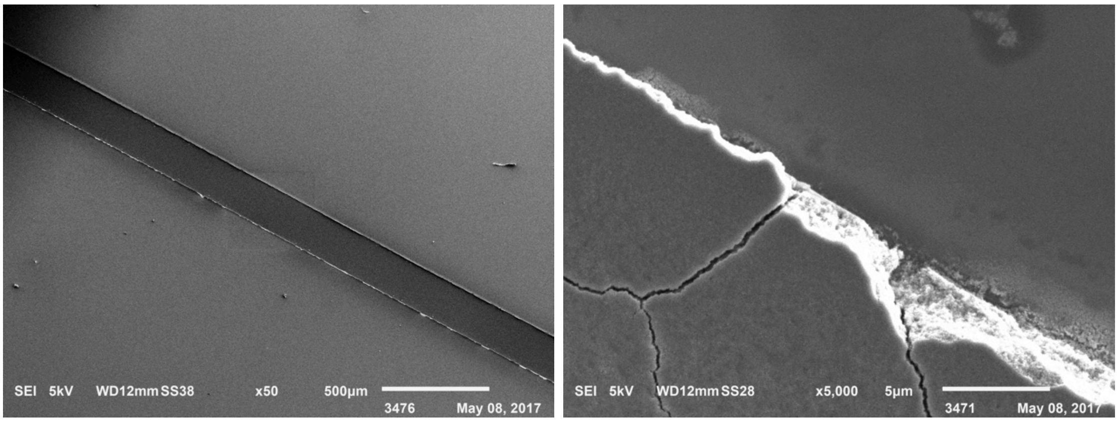

Figure 2.12 SEM images of the stripe with width of 200µm under the magnification of 1) ×50, 2) ×5000.

After patterned with photoresist by photolithography, the wafer was dip coated directly with $TiO_2$ suspension. An uncoated Si strip of 200µm width is shown in Figure 2.12. The rest part is still nicely coated while the edges are not as uniform as the rest part. There are a lot of cracks along the edges due to their high thicknesses.

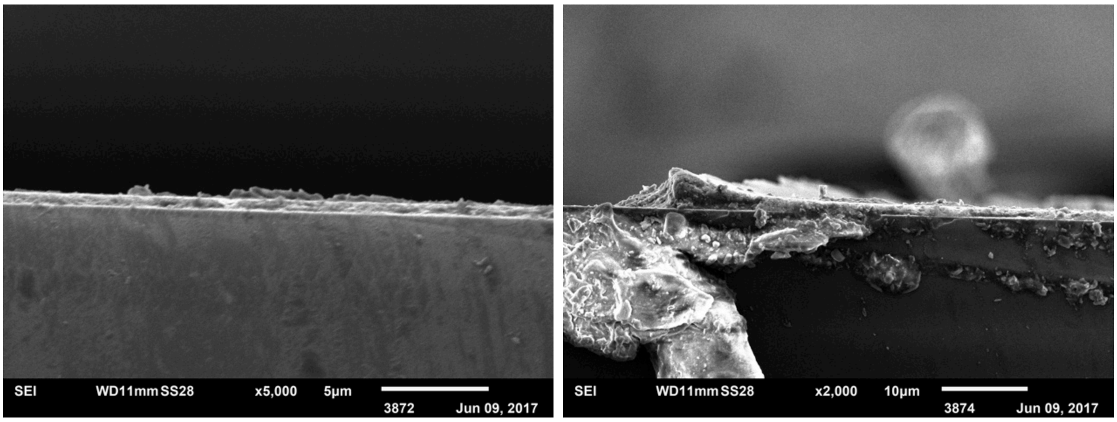

Figure 2.13 Cross sectional SEM images of middle and edge part on a same wafer under the magnification of 1) ×5000, 2) ×2000.

From the left cross sectional images, we can see that the thickness of thin catalyst layer is between 0.5 and 1µm. The edges can be twice or even three times thicker then the rest part.

*Photolithography for Cr coating*

To improve the resolution and uniformity of our patterns, Cr layer was used as the mask for hydrophobization due to its low thickness comparing to the photoresist layer. It was also expected that the Cr layer would give the possibility of surface cleaning before hydrophobization. A thin Cr layer was patterned by photolithography. After hydrophobization, the layer was then etched away with chromium etchant. After this step, some white spots were left on the surface and could not be washed away by nitric acid. The cleaning procedure of nitric acid was changed to $H_2/O_2$ plasma to solve this problem. The hydrophobicity was not high enough for dip coating and the hydrophobic parts were coated with particle clusters. One possible reason is that FOTS layer hydrolyzed in water with the presence of chromium etchant.

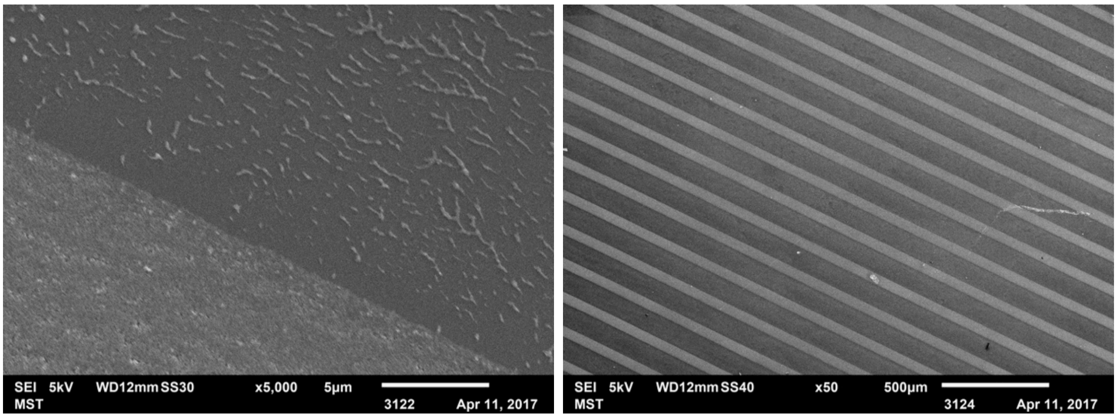

Figure 2.14 SEM images of the stripes with width of 50μm and space length of 100μm under the magnification of 1) ×5000, 2) ×50.

*Photolithography for hydrophobization*

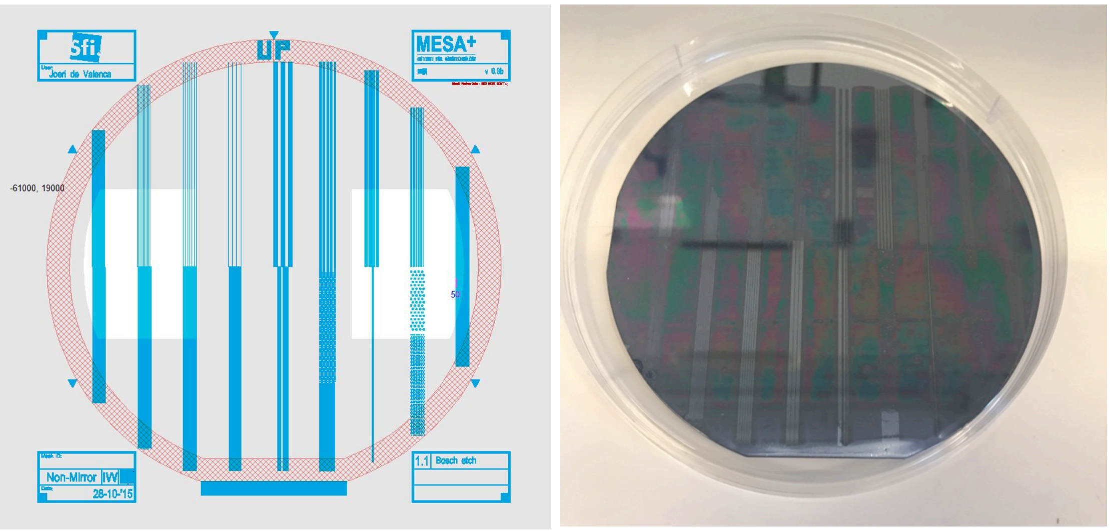

Figure 2.15 Left: Patterns used for photolithography; Right: Dip coated wafer after calcination.

Figure 2.15 shows the mask used for this process. Blue patterns were exposed to photoresist and the rest part of the wafer was covered by the mask. After hydrophobization and lift-off with photoresist, the blue patterns become hydrophobic while the rest part remains hydrophilic. From the pictures taken after calcination, the hydrophobic parts are not coated by the suspension and the strips can be easily recognized. The patterns are checked under SEM for uniformity and resolution.

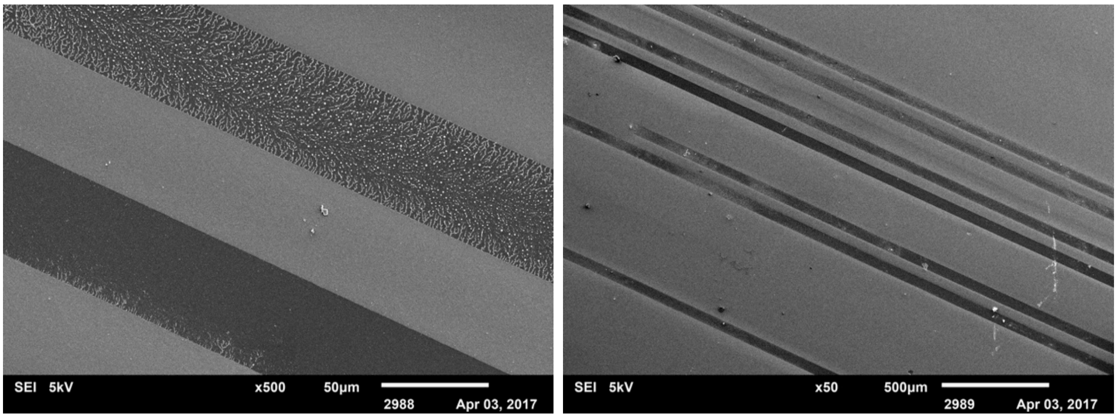

Figure 2.16 SEM images of the stripes with width of 50μm and space length of 50μm under the magnification of 1) ×500, 2) ×50.

From SEM pictures, we can see that the strips with the smallest width of 50μm can be still nicely recognized as well as the rectangles with width of 50μm. However, some of those strips and most of the rectangles are missing.

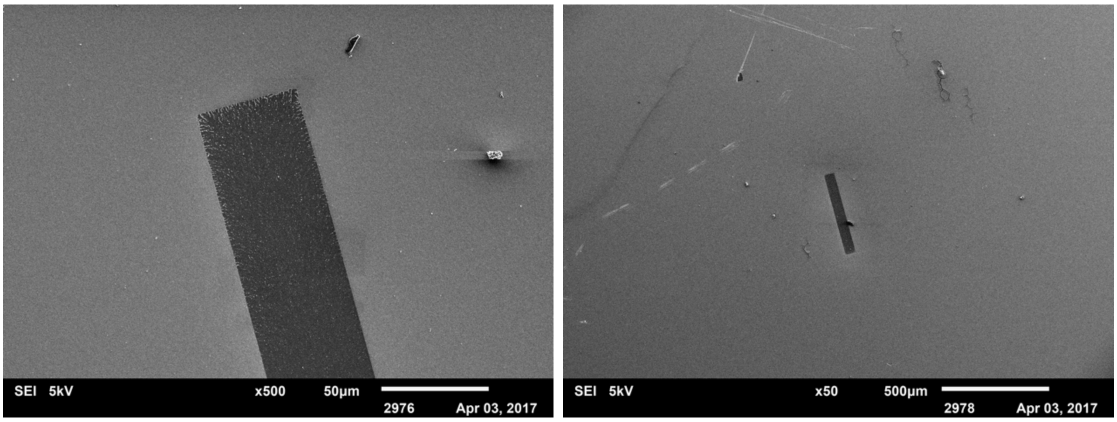

Figure2.17 SEM images of the rectangle with width of 50μm and length of 400μm under the magnification of 1) ×500, 2) ×50.

A large wafer with hydrophilic stripes of different widths was coated to check the resolution of this coating method.

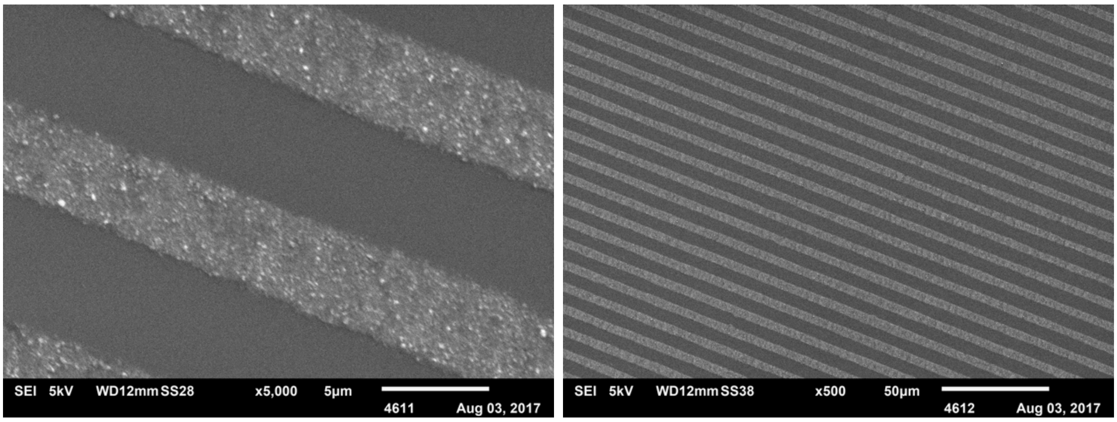

Figure 2.18 SEM images of the strips with width of 5μm under the magnification of 1) ×5000, 2) ×500.

As we can see from the SEM images, $TiO_2$ only selectively coated the hydrophilic part when the lines are 5μm wide. The edges are still clean, but a little rough comparing to those wider lines. Moreover, Figure 2.18 indicated that the catalyst layer is thinner when the size of patterns is smaller. As a result of this experiment, a resolution of 5μm can be easily achieved through dip coating after photolithography for hydrophobization. If we want to have similar thickness of different sizes of patterns, some adjustment needs to be done to the dip coating program.

# Chapter 3

# Biomass Conversion

## 3.1 Theory

### *3.1.1 Fructose to HMF*

Fructose is a simple ketonic monosaccharide, which is often bonded to glucose to form the disaccharide sucrose in many plants. It is frequently derived from sugar, sugar beets and maize. [27] As the main component of sucrose, fructose can be derived from food waste and other biomass resources. Hydrolyzation from sucrose to glucose and fructose can be described as the following equation[28]:

$$C_{12}H_{22}O_{11} + H_2O \rightarrow 2C_6H_{12}O_6$$

Sucrose is not the only source of fructose. Researchers have developed biocatalysts to convert fructose from cellulose[29], which is one of the major component of most plants[30] and agriculture wastes[30]. This is why an environmental-friendly process with a high fructose conversion rate is in strong demand in the biomass conversion industry.

The primary product of the dehydration of fructose is 5-hydroxymethyl-2-furaldehyde (HMF). HMF is a versatile and promising compound. It can be used as a renewable intermediate for the production of polymers, fuels or solvents in the petrochemical industry.

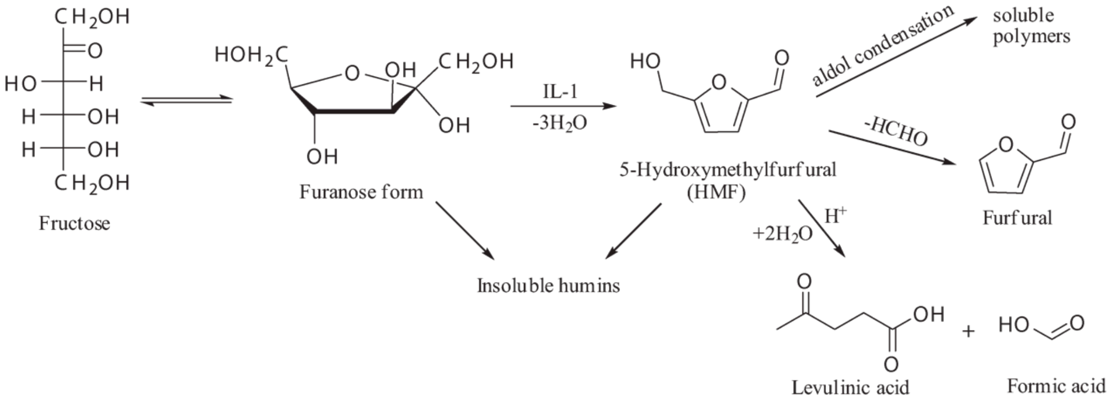

Figure 3.1 A typical reaction scheme for HMF production from fructose. [2]

Solid acids such as oxides[9,14,15], phosphates[31] and chlorides[32,33] have been studied as the catalyst for hydration of fructose. In this assignment, $TiO_2$ and $ZrO_2$ were used to catalyze hexoses dehydration into HMF with their acid sites.[34] Distilled water is used as the medium for its low cost, high sugar solubility and inexistence of media toxicity.[34] High temperature and high pressure are applied to increase the speed and selectivity of this conversion. [14]

It has been proved that metal oxides treated with phosphoric acid have a higher density of acid sites and display an enhanced acid strength, thus improve the dehydration from fructose to HMF.[15,34] After modified with phosphoric acid, -OH groups on $TiO_2$ are esterified into -O-PO($OH_2$) and increase the HMF selectivity.[9,15] What's more, $TiO_2$ exhibits super-hydrophilicity during and after UV light due to the formation of excess surface –OH groups under light irradiation. The combination of UV light and phosphoric acid treatment would increase the density of surface phosphate species, thereby enhancing the catalytic performance.[9]

### *3.1.2 UV-vis spectroscopy*

High performance liquid chromatography (HPLC) is most commonly for the analysis of HMF.[10,14,15,35] With HPLC, the final product after a certain conversion time is measured for the concentration. However, we would like to have a continuous measurement of the conversion with our microreactors. Measuring with HPLC during the experiment is time consuming and inconvenient. Therefore, UV-vis spectroscopy is used to have a real-time measurement on the conversion. HMF as a peak around 284nm in its UV-vis spectrum which was also observed during the measurements. [36]

## 3.2 Experiment

### *3.2.1 Phosphoric acid treatment under UV light*

(i) Chemicals

Phosphoric acid solution ($H_3PO_4$, 85wt% in $H_2O$, SIGMA-ALDRICH), Distilled water.

(ii) Equipment

Pump (Harvard PHD ULTR), UV curer (Egger).

(iii) Procedure

After coated with $TiO_2$, the microchannels were flushed with 1M $H_3PO_4$ solution for 15 min at 50μl/min. While filled with $H_3PO_4$ solution, the microreactors were fixed under UV light for certain duration. After treatment, the microchannels were cleaned by washing away the remaining $H_3PO_4$ solution with distilled water.

### 3.2.2 Conversion from fructose to HMF

(i) Chemicals

D-(-)-Fructose (>99%, SIGMA-ALDRICH), 2-Propanol (EMSURE).

(ii) Equipment

UV-VIS-NIR lightsource (Ocean optics, DT-MINI-2-GS),

(iii) Procedure

Figure 3.2 shows the set up used for this conversion. After flow rate reached a steady state, the microreactor was heated to the set temperature. In the end of each measurement, the microreacter was cooled down in air to stop the reaction and then washed with distilled water and isopropanol.

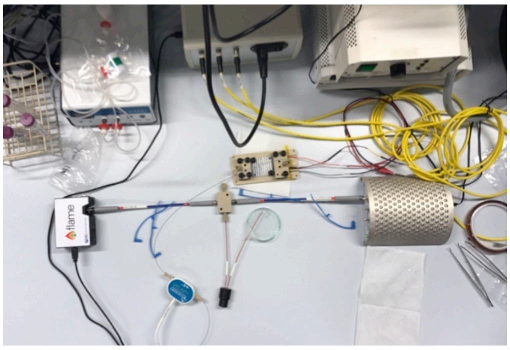

Figure 3.2 Set up used for biomass conversion.

## 3.3 Results and discussion

### 3.3.1 $ZrO_2$ sputtered layer

The performance of dense $ZrO_2$ layer prepared by sputtered deposition was studied.

Table 1. Performance of dense $ZrO_2$ layer prepared by sputtered deposition.

| Fructose concentration (g/L) | 0.5 | | | 1 | |
|---|---|---|---|---|---|
| Flow rate (μl/min) | 0.6 | 0.8 | 1 | 0.8 | 1 |
| Absorbance | 0.121 | 0.028 | 0.012 | 0.892 | 0.696 |
| HMF concentration (mg/L) | 1.00 | 0.231 | 0.100 | 7.37 | 5.75 |
| Product yield (%) | 0.286 | 0.066 | 0.029 | 1.05 | 0.821 |

All the measurements were performed under 135°C and 7bar.

Calibration of HMF was done by my supervisor in advance to get the conversion rate and product yield. From the calibration, we got the following equation:

$$A_{HMF,278.50} = 0.121 \times concentration \tag{1}$$

Product yield was evaluated according to the equations:[14,35]

$$Product\ yield = \frac{an\ amount\ of\ carbon\ atom\ in\ a\ product}{the\ amount\ of\ carbon\ atom\ in\ the\ loaded\ fructose} \times 100$$

$$= \left(\frac{M_f}{M_h}\right)\left(\frac{\#C_h}{\#C_f}\right)\left(\frac{[h]}{[f]_0}\right) \times 100 \qquad (2)$$

$M_f$ is fructose mass molar (180.16 g/mol), $M_h$ is HMF mass molar (126.11 g/mol). $\#C_f$ is carbon numbers of fructose molecule (6), $\#C_h$ is carbon numbers of product HMF molecule (6). $[f]_0$ is fructose initial concentration and $[h]$ is HMF final concentration.

Product yield increased significantly when the concentration of fructose doubled. For each concentration, decreasing flow rate increased the conversion rate. Overall, the conversion rate of $ZrO_2$ sputtered film is too low for commercial use. The reason for that is the low surface area of this catalyst layer. During sputtering, $ZrO_2$ molecules deposit one by one, forming a dense layer. With wash coating and dip coating, we expected to obtain thicker porous layers with larger surface area which can give higher conversion.

### *3.3.2 $ZrO_2$ sputtered layer with patterns*

Four patterned microreactors with different dimensions were tested under the same condition to study how the conversion is influenced by the contrast in reactivity. The catalyst patterns and the distance between them are kept the same to ensure an equal surface catalyst area for the different reactors. Another microchannel coated by a continuous layer that has the same surface area was used as a control group.

Table 3.1 Performance of patterned $ZrO_2$ microchannels.

| Microreactor | Continuous layer | Pattern 1 | Pattern 2 | Pattern3 | Pattern4 |
|---|---|---|---|---|---|
| Space length (μm) | 0 | 400 | 200 | 100 | 50 |
| Absorbance | 0.665 | 0.412 | 0.117 | 0.041 | 0.436 |
| HMF concentration (mg/L) | 5.50 | 3.40 | 0.967 | 0.339 | 3.60 |
| Product yield (%) | 0.786 | 0.486 | 0.138 | 0.048 | 0.514 |

A fructose concentration of 1g/L and a flow rate of 1μl/min were used for all the measurements. Temperature and pressure remained 135°C and 7bar.

Among the four patterned microreactors, pattern1 has the largest dimension while pattern4 has the smallest one. Contrary to our expectation, the conversion rate decreased except for pattern 4. The expectation was that the patterned catalyst would generate an additional transport mechanism. The contrast in reactivity between the active and inactive patches would lead to steep concentration gradients which has been shown to generate surface flows. No clear trend could be concluded from these experiments. It seems that the carbon deposition on the inactive regions is affecting the overall conversion in a more significant degree than any other phenomena that we could speculate on. The small conversion is also an indication for an insignificant diffusion-osmotic flow.

### *3.3.3 $TiO_2$ after phosphoric acid treatment for kinetic study*

The next step is to try to increase the conversion rate by increasing the catalyst surface area. A long straight microchannel wash coated with $TiO_2$ which was treated with phosphoric acid under UV for 4 hours was used for kinetic study.

Table 3.2 Performance of wash-coated $TiO_2$ layer after 4h phosphoric acid treatment with different flow rate.

| Flow rate (μl/min) | 0.2 (saturated) | 0.4 | 0.6 | 0.8 | 1 |
|---|---|---|---|---|---|
| Absorbance | 1.826 | 1.428 | 0.951 | 0.492 | 0.370 |
| HMF concentration (mg/L) | 15.1 | 11.8 | 7.86 | 4.07 | 3.06 |
| Product yield (%) | 4.31 | 3.37 | 2.25 | 1.16 | 0.874 |

A fructose solution of 0.5 g/L was used for the five measurements. Pressure remained 7 bar while temperature was reduced to 130°C, because the temperature difference between the middle and the edges of this long straight channel is around 5°C.

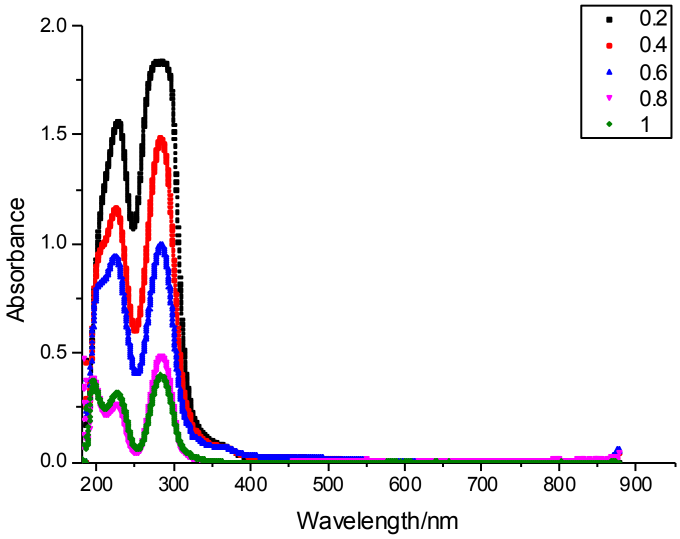

Figure 3.3 Full spectrums of the final state of the conversion at different flow rates.

When the flow rate is increased, the residence time is reduced and so is the conversion. Figure 3.3 shows the full spectra of the steady states of each measurement. Unlike the others, the full spectra at 0.2μl/min has a much broader peak around 284nm. It is highly possible that the signal is saturated and could not go any higher, which means we had a higher product yield than 4.31%. This is why the data under saturated condition are not used in fitting the kinetics.

Since the product yield is so low, intrinsic react rate is barely influenced by mass transfer. Therefore we can calculate the reaction rate constant by using a plug flow reactor equation. The reaction is assumend to be first order and all the fructose to be converted into HMF.

$$\frac{d[f]}{dt} = -k[f] \tag{3}$$

$$ln\frac{[f]_0}{[f]} = ln\frac{[f]_0}{[f]_0-[h]} = kt \tag{4}$$

By linear fitting, we got the reaction rate coefficient k of 0.00634 $\text{min}^{-1}$ for this $TiO_2$ wash coated catalyst.

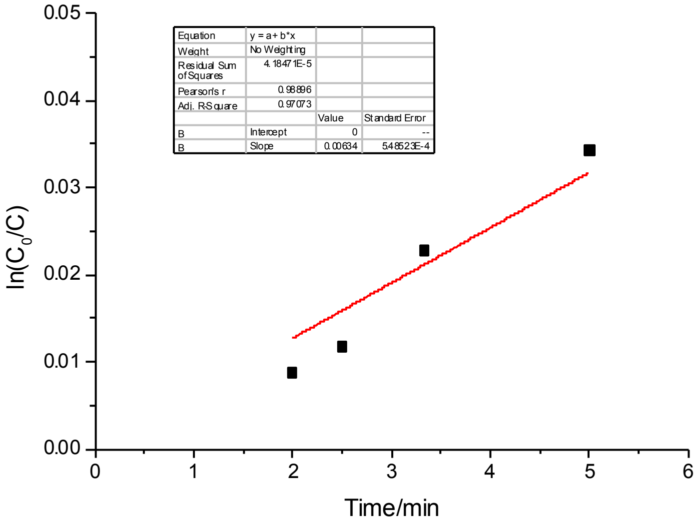

Figure 3.4 Fitting line for reaction rate coefficient.

### 3.3.4 $TiO_2$ after phosphoric acid treatment for temperature study

Another microchannel was prepared for temperature study by treatment with phosphoric acid for 6 hours.

Table 3.3 Performance of wash-coated $TiO_2$ layer after 6h phosphoric acid treatment with different temperature.

| Temperature (°C) | 100 | 110 | 120 | 130 (saturated) |
|---|---|---|---|---|
| Absorbance | 0.021 | 0.262 | 1.402 | 1.901 |
| HMF concentration (mg/L) | 0.174 | 2.17 | 11.6 | 15.7 |
| Product yield (%) | 0.0497 | 0.620 | 3.31 | 4.49 |

All the measurements were done with a 0.5g/L fructose solution at the flow rate of 0.4µl/min.

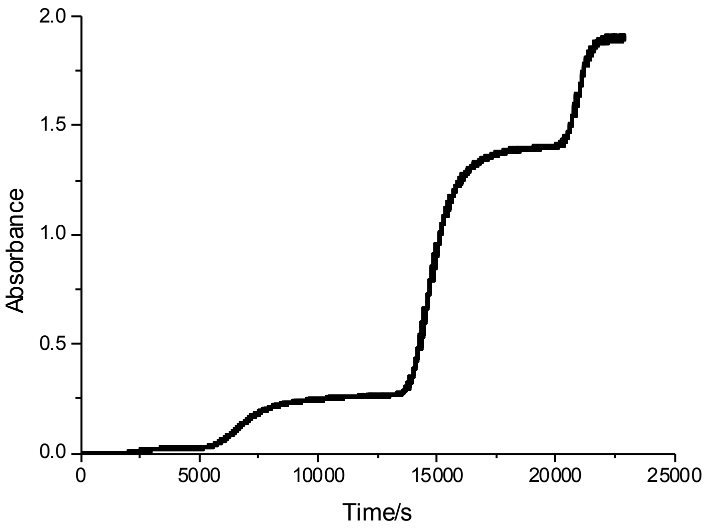

Figure 3.5 Absorbance curve during the measurement with four temperature steps.

Figure 3.5 shows the conversion already started at 100°C. At 130°C, the signal of HMF is saturated again and does not show the real concentration.

The activation energy can be derived from the Arrhenius equation:

$$k = Ae^{-E_a/RT} \tag{5}$$

$$E_a \cdot \frac{1}{RT} - \ln A = -\ln k \tag{6}$$

The reaction rate constants that were obtained using equation 4 are shown as below:

Table 3.4 Reaction rate constant at each temperature.

| Temperature (°C) | 100 | 110 | 120 | 130 |
|---|---|---|---|---|
| k ($\text{min}^{-1}$) | $9.92\times10^{-5}$ | 0.00124 | 0.00673 | 0.00918 |

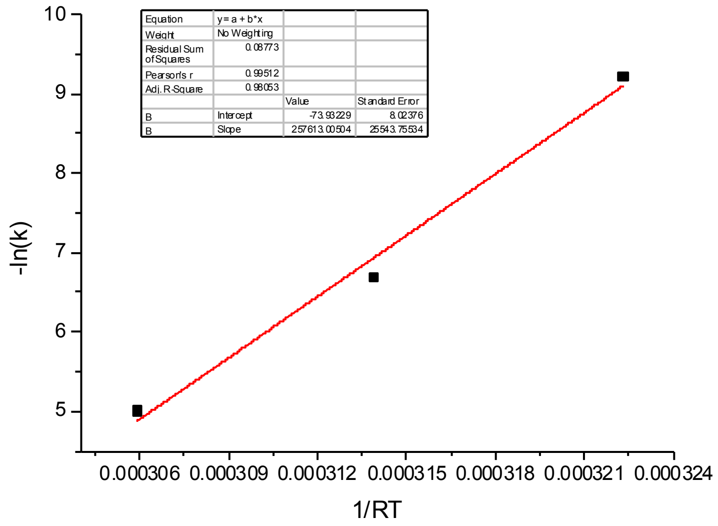

Figure 21. Fitting line for activation energy.

By fitting, we got the activation energy of 258kJ/mol.

### *3.3.5 Comparison between different microreactors*

For the second part of this assignment, we tested two different kinds of catalyst films in total: sputtered $ZrO_2$ dense thin film and wash coated $TiO_2$ porous thick film. Two $TiO_2$ coated microchannels were treated with phosphoric acid for different durations. The results are concluded into the following table:

Table 3.5 Performance comparisons between three different microchannels.

| | $ZrO_2$ | $TiO_2$ (4h treatment) | $TiO_2$ (6h treatment) |
|---|---|---|---|
| Microchannel volume (μl) | 4.5 | 2 | 2 |
| Flow rate (μl/min) | 0.8 | 0.4 | 0.4 |
| Resistance time (min) | 5.625 | 5 | 5 |
| Fructose concentration (g/L) | 0.5 | 0.5 | 0.5 |
| Pressure (bar) | 7 | 7 | 7 |
| Temperature (°C) | 135 | 130 | 130 |
| Product yield (%) | 0.066 | 3.37 | >4.49 |

With lower temperature and residence time, wash-coated $TiO_2$ has more than 50 times higher product yield than the sputtered $ZrO_2$ layer. The conversion is further enhanced when we prolonged the phosphoric acid treatment. In conclusion, larger surface area and phosphoric acid treatment are effective ways to promote the conversion from fructose to HMF.

# Chapter 4

# Conclusion

In this assignment, a simple and straight-forward method to pattern thick porous catalyst on Si substrate using contrast in wettability was introduced. Si wafers were hydrophobized after photolithography for dip coating. Strips with minimum width of 5μm were successfully patterned with sharp boundaries and homogenous surface. This method can be used for patterning porous catalyst inside microchannels.

Then the kinetic process of a biomass conversion from fructose to 5-hydroxymethyl-2-furaldehyde (HMF) was studied using UV-vis spectroscopy. Both sputtered $ZrO_2$ layer and wash coated $TiO_2$ layer were tested under different flow rate, temperature and fructose solution concentration. Phosphoric acid treatment under UV light was also applied to the porous $TiO_2$ catalyst to enhance the product yield. As shown in the results, enlarging surface area of the catalyst film and using phosphoric acid treatment can both significantly improve the performance of the microreactor.

The initial idea of the project regarding mass transfer enhancement could not be met due to the slow kinetics. The small reaction rate is the limiting step in the overall conversion process, making the mass transfer rate irrelevant. Furthermore, the concentration gradients between the active and inactive patterns are believed to be small, making the diffusio-osmotic flow insignificant. A catalyst with a much higher activity is needed for this surface flow generation study.

# Chapter 5

# Recommendation

UV-vis spectroscopy only shows the concentration of HMF after conversion. However, it is highly possible that HMF is not the only product from fructose. Potential by products include levulinic acid, formic acid and glucose. Total amount of converted fructose is necessary to calculate conversion rate and selectivity of the catalyst. Therefore, the outlet liquid can be collected and examined by HPLC after the highest conversion is reached.

For the fabrication part, catalyst patterns are too small to be measured with ellipsometry. Atomic force microscopy can be used to measure the surface structure of these patterns, including layer thickness and surface homogeneity.

Product yield can be further improved by increasing the system pressure and temperature, as well as the phosphoric acid treatment duration. A water-immiscible organic phase, for example tetrahydrofuran (THF), can be used to extract HMF from the aqueous phase, in order to shift the reaction to the right side and prevent the quick degradation of HMF into undesired by-products. [15,37]

# Reference

[1] Ulman A. Formation and Structure of Self-Assembled Monolayers. *Chemical Reviews* **1996**, 96 (4), 1533-54.

[2] Tao F, Song H, Chou L. Dehydration of fructose into 5-hydroxymethylfurfural in acidic ionic liquids. *RSC Advance* **2011**, 1, 672-6.

[3] Mohseni E, Zalnezhad E, Bushroa AR. Comparative investigation on the adhesion of hydroxyapatite coating on Ti–6Al–4V implant: A review paper. *International Journal of Adhesion and Adhesives* **2014**, 48, 238-57.

[4] Wikipedia. Biomass. https://en.wikipedia.org/wiki/Biomass.

[5] Huber GW, Iborra S, Corma A. Synthesis of Transportation Fuels from Biomass- Chemistry, Catalysts, and Engineering. *Chemical Reviews* **2006**, 106, 4044-98.

[6] Demirbas A. Biomass resource facilities and biomass conversion processing for fuels and chemicals. *Energy Conversion and Management* **2001**, 42 (11), 1357-78.

[7] Du XL, Bi QY, Liu YM, Cao Y, Fan KN. Conversion of biomass-derived levulinate and formate esters into gamma-valerolactone over supported gold catalysts. *ChemSusChem* **2011**, 4 (12), 1838-43.

[8] Tang X, Chen H, Hu L, et al. Conversion of biomass to γ-valerolactone by catalytic transfer hydrogenation of ethyl levulinate over metal hydroxides. *Applied Catalysis B: Environmental* **2014**, 147, 827-34.

[9] Hattori M, Kamata K, Hara M. Photoassist-phosphorylated TiO2 as a catalyst for direct formation of 5-(hydroxymethyl)furfural from glucose. *Phys Chem Chem Phys* **2017**, 19 (5), 3688-93.

[10] de Souza RL, Yu H, Rataboul F, Essayem N. 5-Hydroxymethylfurfural (5-HMF) Production from Hexoses: Limits of Heterogeneous Catalysis in Hydrothermal Conditions and Potential of Concentrated Aqueous Organic Acids as Reactive Solvent System. *Challenges* **2012**, 3 (2), 212-32.

[11] Du XL, He L, Zhao S, et al. Hydrogen-independent reductive transformation of carbohydrate biomass into gamma-valerolactone and pyrrolidone derivatives with supported gold catalysts. *Angew Chem Int Ed Engl* **2011**, 50 (34), 7815-9.

[12] Yan K, Chen A. Selective hydrogenation of furfural and levulinic acid to biofuels on the ecofriendly Cu–Fe catalyst. *Fuel* **2014**, 115, 101-8.

[13] Chia M, Dumesic JA. Liquid-phase catalytic transfer hydrogenation and cyclization of levulinic acid and its esters to gamma-valerolactone over metal oxide catalysts. *Chem Commun (Camb)* **2011**, 47 (44), 12233-5.

[14] Watanabe M, Aizawa Y, Iida T, Nishimura R, Inomata H. Catalytic glucose and fructose conversions with TiO2 and ZrO2 in water at 473K: Relationship

between reactivity and acid–base property determined by TPD measurement. *Applied Catalysis A: General* **2005**, 295 (2), 150-6.

[15] Nakajima K, Noma R, Kitano M, Hara M. Selective glucose transformation by titania as a heterogeneous Lewis acid catalyst. *Journal of Molecular Catalysis A: Chemical* **2014**, 388-389, 100-5.

[16] Wikipedia. Microreactor. https://en.wikipedia.org/wiki/Microreactor.

[17] Mills PL, Quiram DJ, Ryley JF. Microreactor technology and process miniaturization for catalytic reactions—A perspective on recent developments and emerging technologies. *Chemical Engineering Science* **2007**, 62 (24), 6992-7010.

[18] Wan YSS, Chau JLH, Gavriilidis A, Yeung KL. Design and fabrication of zeolite-based microreactors and membrane microseparators. *Microporous and Mesoporous Materials* **2001**, 42 (2-3), 157-75.

[19] Kanamori Y, Kaneko A, Moronuki N, Kubo T. Self-Assembly of Fine Particles on Patterned Wettability in Dip Coating and Its Scale Extension with Contact Printing. *Journal of Advanced Mechanical Design, Systems, and Manufacturing* **2008**, 2 (4), 783-91.

[20] Heule M, Schönholzer UP, Gauckler LJ. Patterning colloidal suspensions by selective wetting of microcontact-printed surfaces. *Journal of the European Ceramic Society* **2004**, 24 (9), 2733-9.

[21] Knieling T, Lang W, Benecke W. Gas phase hydrophobisation of MEMS silicon structures with self-assembling monolayers for avoiding in-use sticking. *Sensors and Actuators B: Chemical* **2007**, 126 (1), 13-7.

[22] Pennemann H, Dobra M, Wichert M, Kolb G. Optimization of Wash-Coating Slurries as Catalyst Carrier for Screen Printing into Microstructured Reactors. *Chemical Engineering & Technology* **2013**, 36 (6), 1033-41.

[23] McDonnell AMP, Beving D, Wang A, Chen W, Yan Y. Hydrophilic and Antimicrobial Zeolite Coatings for Gravity-Independent Water Separation. *Advanced Functional Materials* **2005**, 15 (2), 336-40.

[24] D'Angelo MF, Ordomsky V, Paunovic V, van der Schaaf J, Schouten JC, Nijhuis TA. Hydrogen production through aqueous-phase reforming of ethylene glycol in a washcoated microchannel. *ChemSusChem* **2013**, 6 (9), 1708-16.

[25] Meille V. Review on methods to deposit catalysts on structured surfaces. *Applied Catalysis A: General* **2006**, 315, 1-17.

[26] Brinker CJ, Frye GC, Hurd AJ, Ashley CS. Fundamentals of Sol-Gel Dip Coating. *Thin Solid Films* **1991**, 201, 97-108.

[27] Wikipedia. Fructose. https://en.wikipedia.org/wiki/Fructose.

[28] Halford NG. An Introduction to Bioenergy; 2014.

[29] Lee Y-C, Chen C-T, Chiu Y-T, Wu KCW. An Effective Cellulose-to-Glucose-to-Fructose Conversion Sequence by Using Enzyme Immobilized Fe3O4-Loaded Mesoporous Silica Nanoparticles as Recyclable

Biocatalysts. *ChemCatChem* **2013**, 5 (8), 2153-7.

[30] Saini JK, Saini R, Tewari L. Lignocellulosic agriculture wastes as biomass feedstocks for second-generation bioethanol production: concepts and recent developments. *3 Biotech* **2015**, 5 (4), 337-53.

[31] Ordomsky VV, Sushkevich VL, Schouten JC, van der Schaaf J, Nijhuis TA. Glucose dehydration to 5-hydroxymethylfurfural over phosphate catalysts. *Journal of Catalysis* **2013**, 300, 37-46.

[32] Pagán-Torres YJ, Wang T, Gallo JMR, Shanks BH, Dumesic JA. Production of 5-Hydroxymethylfurfural from Glucose Using a Combination of Lewis and Brønsted Acid Catalysts in Water in a Biphasic Reactor with an Alkylphenol Solvent. *ACS Catalysis* **2012**, 2 (6), 930-4.

[33] Zhao H, Holladay JE, Brown H, Zhang ZC. Metal chlorides in ionic liquid solvents convert sugars to 5-hydroxymethylfurfural. *Science* **2007**, 316 (5831), 1597-600.

[34] Siqueira BG, Silva MAP, Moraes C. Synthesis of Hmf from Glucose in Aqueous Medium Using Niobium and Titanium Oxides. *Brazilian Journal of Petroleum and Gas* **2013**, 7 (2), 71-82.

[35] Lanziano CS, Rodriguez F, Rabelo SC, Guirardello R, da Silva VT, Rodella CB. Catalytic Conversion of Glucose Using TiO2 Catalysts. *Chemical Engineering Transactions* **2014**, 37, 589-94.

[36] Zhang J, Li J, Tang Y, Xue G. Rapid method for the determination of 5-hydroxymethylfurfural and levulinic acid using a double-wavelength UV spectroscopy. *ScientificWorldJournal* **2013**, 2013, 506329.

[37] Nikolla E, Román-Leshkov Y, Moliner M, Davis ME. “One-Pot” Synthesis of 5-(Hydroxymethyl)furfural from Carbohydrates using Tin-Beta Zeolite. *ACS Catalysis* **2011**, 1 (4), 408-10.